Proceedings of the ASME Turbo Expo 2022
Turbomachinery Technical Conference and Exposition
GT2022
June 13-17, 2022, Rotterdam, The Netherlands

GT2022-82931

QUANTIFICATION OF AUTOIGNITION RISK IN AERODERIVATIVE GAS TURBINE PREMIXERS USING INCOMPLETELY STIRRED REACTOR AND SURROGATE MODELLING

Salvatore Iavarone[1,2,*], Savvas Gkantonas[1], Sandeep Jella[3], Philippe Versailles[3], Sajjad Yousefian[4,5,6], Rory F. D. Monaghan[4,5,6], Epaminondas Mastorakos[1], Gilles Bourque[3]

[1]Department of Engineering, University of Cambridge, Cambridge, United Kingdom
[2]Aero-Thermo-Mechanics Laboratory, École polytechnique de Bruxelles, Université Libre de Bruxelles, Brussels, Belgium
[3]Siemens Energy Canada Ltd, 9545 Côte-de-Liesse Road, Montréal, Québec, Canada
[4]MaREI Centre for Energy, Climate and Marine, Ireland
[5]Combustion Chemistry Centre, National University of Ireland, Galway Ireland
[6]School of Engineering, National University of Ireland Galway, Ireland

ABSTRACT

The design and operation of premixers for gas turbines must deal with the possibility of relatively rare events causing dangerous autoignition. Rare autoignition events may occur in the presence of fluctuations of operational parameters, such as temperature and fuel composition, and must be understood and predicted. This work presents a methodology based on Incompletely Stirred Reactor (ISR) and surrogate modelling to increase efficiency and feasibility in premixer design optimisation for rare events. For a representative premixer, a space-filling design is used to sample the variability of three influential operational parameters. An ISR is then reconstructed and solved in a post-processing fashion for each sample, leveraging a well-resolved CFD solution of the non-reacting flow inside the premixer. Via detailed chemistry and reduced computational costs, the evolution of autoignition precursors and temperature, conditioned on a mixture fraction, is tracked, and accurate surrogate models are trained on all samples. The final quantification of the autoignition probability is achieved by querying the surrogate models via Monte Carlo sampling of the random parameters. The approach is fast and reliable so that user-controllable, independent variables can be optimised to maximise system performance while observing a constraint on the allowable probability of autoignition.

Keywords: Autoignition, Gas Turbine Premixers, Surrogate modelling, Stochastic modelling

1. INTRODUCTION

In typical gas turbines aiming to achieve lean premixed combustion, the design and operation of premixers focus on achieving residence times low enough to prevent autoignition, but high enough to obtain adequate mixing. Premixers are designed to obtain residence time distributions that are at least two orders of magnitude below typical ignition delays [1]. However, at engine conditions, intermediate radicals are formed even at these short time-scales and if their reactions are able to progress to a critical point determined by local mixture concentration, residence time, temperature and turbulent mixing rates, ignition kernels with localised heat release can form and rapidly lead to a propagating flame in the premixer [2, 3]. Thus, rare autoignition events may occur in the presence of fluctuations of various physical quantities and must be understood and predicted.

Computational Fluid Dynamics (CFD) simulations can be employed to improve the understanding of the autoignition process inside a premixer. These simulations must feature an accurate description of the turbulent mixing process and a detailed chemical mechanism that can properly model reaction pathways of low-temperature precursors (e.g., H_2O_2) at high pressures [4]. However, a significant number of simulations at different operating conditions may be required to design premixers and compute the probability of rare autoignition events, all using detailed chemistry. Autoignition may be caused by the variability of the initial operating conditions of the premixer, and a strategy to compute its probability is to sample a large number of conditions from the distribution that defines their uncertainty, propagate the system in time, and count the number of samples that lead to autoignition. This procedure is carried out by so-called *forward* Uncertainty Quantification approaches, which determine the uncertainty in the prediction of selected quantities of interest due to known variability of input and/or model parameters, usually described by probability density functions. In combustion studies, forward propagation of uncertainties provided prediction intervals on laminar flame speeds [5, 6], ignition delay times [7, 8], and

*Corresponding author: si339@cam.ac.uk

NO_x emissions [9–11]. Monte-Carlo methods provide the most direct approach to propagating uncertainties and estimating the variability in the predictions, although they require a significant number of realisations. Thus, Monte-Carlo methods are computationally unfeasible when the realisations are obtained by CFD simulations due to their high dimensionality and computational cost. Several studies focused on solving these issues by either reducing the number of samples needed to accurately compute the output probability density functions [12–14] or using surrogate models or meta-models [15–18], which are low-order functions constructed (trained) upon a reduced number of CFD simulations. In the latter case, the training of accurate surrogate models may be still hindered by the high dimensionality of the uncertain parameter space and the computational cost of the several CFD simulations needed. Thus, a crucial need exists to develop and employ computationally inexpensive methods that simplify calculations with detailed turbulence and chemistry models, provide predictions within a reasonable degree of accuracy, and capture system responses to perturbations and, eventually, rare events.

This work presents a methodology based on Incompletely Stirred Reactor (ISR) and surrogate modelling to quantify autoignition risk in aeroderivative gas turbine premixers accurately and with low computational costs. The ISR modelling removes the need to perform many computationally expensive reacting flow simulations by relying only on one well-resolved CFD simulation of the inert flow, which is then kinetically post-processed. A surrogate model, trained on several ISR simulations of a premixer, then aims to compute the probability of autoignition kernel formation and thus quantify the autoignition risk in the premixer due to the variability of its operational parameters.

An ISR can be defined here as the premixer volume within which conditional averages of reacting scalars, conditioned on a mixture fraction that denotes fuel/air mixing, are homogeneous but with the flow and mixture fraction being inhomogeneous. By directly considering the mixing field, featuring the mixture fraction mean and variance and the scalar dissipation rate, provided by a CFD computation, ISR equations are solved for reacting scalars, such as concentrations of autoignition precursors and temperature, so that autoignition metrics can be explicitly analysed and used in a surrogate model. This approach is computationally not expensive since the ISR only involves the solution of a set of ordinary differential equations that are solved in a post-processing fashion, further allowing the use of detailed chemistry. The coupling of CFD with an ISR as a post-processing step is similar to what is typically performed in Chemical Reactor Network approaches using ideal reactors (e.g., see [19] for a review). However, an ISR allows for an elaborate treatment of unmixedness and micromixing effects which are crucial for autoignition and other low Damköhler number phenomena. The ISR theory was first developed by Bilger and coworkers [20–23] on the theoretical foundation laid by the Conditional Moment Closure (CMC) method for turbulent reacting flows [24]. Methods based on ISRs have previously been applied to experimental lab-scale combustors [22, 25], a heavy-duty diesel engine [26] and model aeroengine combustors [27–30] demonstrating good accuracy for predicting gas-phase pollutants and soot. More recently, ISR theory has also been validated as a suitable approach to estimate autoignition propensity. Using a network of ISRs to postprocess non-reacting CFD computations, Iavarone et al. [31] successfully reproduced hydrogen autoignition locations in a turbulent atmospheric co-flow of heated air [3], whereas Gkantonas et al. [32] observed the good performance of the ISR network (ISRN) in capturing the autoignition behaviour inside an aeroderivative gas turbine premixer previously studied with reacting CFD [1]. The same premixer used in [1, 32] is also investigated here. However, this work focuses on predicting the occurrence of autoignition in the premixer, rather than the location of autoignition kernels. For this purpose, a single ISR, rather than a network, is used, enabling stochastic autoignition modelling thanks to its reduced computational costs.

The specific objectives of the present work are to (i) perform stochastic autoignition modelling by considering uncertainties in three influential input quantities, i.e., fuel temperature, air temperature, and fuel mixture composition, used in an ISR representation of a premixer with real-life geometric complexity; (ii) investigate the effect of these quantities on the probability of autoignition; (iii) quantify the autoignition risk in the premixer at different operating conditions. The first objective of the work is carried out by training a surrogate model on several ISR simulations of the premixer. The ISR simulations are carried out in post-processing and take as input the mixing field, provided by a non-reactive CFD simulation of the premixer, and different possible values of the three influential operating conditions. Temperature and species mass fractions, conditioned on the mixture fraction, are obtained as output and provide indications about the occurrence of autoignition in the premixer at the considered conditions. For a selected ISR output, which acts as an autoignition metric, the most accurate response surface, indicating the relationship between the variable and the input parameters, is found by employing and comparing different surrogate-modelling approaches. The second and third objectives are then achieved by querying the surrogate model via Monte Carlo sampling of the random influential input parameters. The paper is structured as follows. The derivation of the ISR equations is first presented, followed by details on the sub-models used in the computations. A brief description of the investigated premixer and the mixing field obtained by a reference CFD simulation is then reported. Next, the solution strategy employed for the stochastic modelling of the premixer is presented. Results and key conclusions close the paper.

2. THE ISR APPROACH

The derivation of the governing equations for an Incompletely Stirred Reactor (ISR), either as a single reactor or as part of a reactor network, is based on the singly-conditioned Conditional Moment Closure (CMC) method presented in various works (e.g., see [24, 30]) and validated for autoignition in several studies [33–36]. The ISR equation may be viewed as a zero-dimensional (or spatially integrated) approximation of the full multi-dimensional CMC equation. The underlying concept is to make the mixture fraction PDF and the scalar dissipation rate, dictating micromixing, appear in the governing equation and consequently extract those quantities from a reference CFD simulation, here describing the non-reacting flow. The ISR equations are solved in a post-

processing fashion so that any chemical mechanism of arbitrary complexity can be used as well as various operating conditions, as considered in Section 4 for three influential input parameters. As the flow and mixing fields are pre-calculated and only a subset of processes are solved, the computational time is drastically reduced compared to a detailed CFD simulation. For the problem of autoignition, where only small density changes are expected to occur before autoignition happens, post-processing non-reacting flow mixing patterns introduces only small errors [4].

2.1 Mathematical model

An ISR is considered to be a volume V (here, the whole premixer volume) within which conditional averages of reacting scalars, conditioned on the mixture fraction, are independent of position. In contrast to a perfectly-stirred reactor, which has a uniform composition, this allows an ISR to have mixture fraction inhomogeneities which are important for autoignition calculations. The partially stirred reactor (PaSR) model, derived from the Monte-Carlo PDF method (e.g., see [37]), has similarities with the ISR model. However, in a PaSR, there is no direct link between the reactor mixing rates and the ones from the flow field. Various versions of the ISR governing equations have appeared in the literature [20–23, 26, 29]. Here, the derivation is presented for completeness.

The equations are derived from the transport equation of the conditional expectation (here considered to be density-weighted and time-averaged) of a generic species α, $Q_\alpha \equiv \langle Y_\alpha|\xi=\eta\rangle$, but also including the mixture fraction PDF, P_η, with η being the sample space variable of the mixture fraction, ξ. Based on [24], the transport equation reads:

$$\frac{\partial \bar{\rho} Q_\alpha P_\eta}{\partial t} + \frac{\partial}{\partial x_i}(\bar{\rho}\langle u_i Y_\alpha|\eta\rangle P_\eta) = -Q_\alpha \frac{\partial^2 \bar{\rho}\langle N|\eta\rangle P_\eta}{\partial \eta^2} + \bar{\rho}\langle N|\eta\rangle P_\eta \frac{\partial^2 Q_\alpha}{\partial \eta^2} + \bar{\rho}\langle \dot{\omega}_\alpha|\eta\rangle P_\eta, \tag{1}$$

where $N \equiv D\vec{\nabla}\xi \cdot \vec{\nabla}\xi$ is the scalar dissipation rate (SDR). Note that differential diffusion effects can be included in Eq. 1 but a unity Lewis number assumption is used here instead since no highly diffusive species are present in the fuel-air mixture (see Section 3).

Considering statistically stationary flow, integration of Eq. 1 over the reactor's volume and the application of the flux divergence theorem to the LHS leads to:

$$\oint_A \bar{\rho}\langle\vec{u}|\eta\rangle Q_\alpha P_\eta \cdot d\vec{A} = -\int_V \left(Q_\alpha \frac{\partial^2 \bar{\rho}\langle N|\eta\rangle P_\eta}{\partial \eta^2}\right) dV + \int_V \left(\bar{\rho}\langle N|\eta\rangle P_\eta \frac{\partial^2 Q_\alpha}{\partial \eta^2} + \bar{\rho}\langle \dot{\omega}_\alpha|\eta\rangle P_\eta\right) dV, \tag{2}$$

In Eq. 2, conditional correlations between reacting scalars and velocity are neglected, so all fluctuations about the conditional mean in the inlet and outlet flows are not considered, consistent with ISR theory [24]. By definition, conditional reactive scalar statistics and their functions, e.g., chemical source terms, are also considered uniform inside an ISR core. Hence, they can be moved out of the integral on the RHS of Eq. 2. This allows for the introduction of the core-averaged mass density, ρ^{**}, mixture fraction PDF, P_η^{**}, and SDR, N_η^{**}, in the equation, which can be computed by CFD simulations after appropriate time-averaging. The core-averaged quantities are given by:

$$\rho^{**} \equiv \frac{\int_V \bar{\rho} dV'}{V}; P_\eta^{**} \equiv \frac{\int_V \bar{\rho} P_\eta dV'}{\rho^{**} V}; N_\eta^{**} \equiv \frac{\int_V \bar{\rho}\langle N|\eta\rangle P_\eta dV'}{\rho^{**} V P_\eta^{**}}. \tag{3}$$

In addition, a mass-flow-rate-weighted mixture fraction PDF for the inlet and outlet streams can be introduced which is given by:

$$P_\eta^* \equiv \frac{1}{\dot{m}} \int_A \bar{\rho}\langle\vec{u}|\eta\rangle P_\eta \cdot d\vec{A}. \tag{4}$$

Combining Eqs. 2–4, the ISR equation then reads:

$$\frac{(Q_\alpha P^*)_{\text{out}} - (Q_\alpha P^*)_{\text{in}}}{\tau_r} = -Q_\alpha \frac{d^2 N_\eta^{**} P_\eta^{**}}{d\eta^2} + P_\eta^{**}\left(N_\eta^{**} \frac{d^2 Q_\alpha}{d\eta^2} + \langle\dot{\omega}_\alpha|\eta\rangle\right), \tag{5}$$

where the reactor residence time, $\tau_r \equiv (\rho^{**}V)/\dot{m}$, has been utilised. Note that the partial derivatives in Eq. 2 have been replaced with ordinary ones in Eq. 5 since conditional statistics are now only a function of the mixture fraction. To close the first term on the RHS of Eq. 5, the transport equation for the mixture fraction PDF may be utilised [24]. If molecular fluxes are neglected, the PDF equation is equivalent to Eq. 1 with $Q_\alpha = 1$ and no chemistry source term. Since Q_α is constant, its derivative is zero. Considering stationary flow, the integration of the PDF equation over the core volume reads:

$$\frac{\oint_A \bar{\rho}\langle\vec{u}|\eta\rangle P_\eta \cdot d\vec{A}}{\rho^{**} V} = \frac{(P_\eta^*)_{\text{out}} - (P_\eta^*)_{\text{in}}}{\tau_r} = -\frac{d^2 N_\eta^{**} P_\eta^{**}}{d\eta^2}, \tag{6}$$

where Eq. 3 and the flux divergence theorem have been applied. Furthermore, to derive the final ISR equation, the conditional averages at the ISR outlet are considered equal to the conditional averages at the core, i.e., $(Q_\alpha)_{\text{out}} = Q_\alpha$, consistent with the stirred reactor concept and discussed in [23]. Consequently, the ISR equation may be derived as follows:

$$\frac{(P_\eta^*)_{\text{in}}}{\tau_r P_\eta^{**}}\left(Q_\alpha - (Q_\alpha)_{\text{in}}\right) = N_\eta^{**} \frac{d^2 Q_\alpha}{d\eta^2} + \langle\dot{\omega}_\alpha|\eta\rangle. \tag{7}$$

In the special case of completely unmixed inlet streams, as in a premixer, the inlet PDF, $(P_\eta^*)_{\text{in}}$, is zero at $0 < \eta < 1$ since only mixture fractions at 0 or 1 are possible, i.e., the inlet PDF consists of two Dirac δ-functions at the mixture fraction space bounds. Considering that Dirichlet conditions are used for the bounds in CMC and ISR equations, then the ISR equation is written as:

$$0 = N_\eta^{**} \frac{d^2 Q_\alpha}{d\eta^2} + \langle\dot{\omega}_\alpha|\eta\rangle. \tag{8}$$

Equation 8 is virtually identical to the steady-state flamelet model for unity Lewis number [38]. Although the core-averaged PDF and residence time do not appear in Eq. 8 directly, they dictate the profile of the core-averaged SDR profile, N_η^{**}. The

latter may be calculated from the double integral of Eq. 6 as follows:

$$N_{\eta}^{**} = \frac{1}{\tau_r P_{\eta}^{**}} \int_0^{\eta} \int_0^{\eta'} \Big((P_{\eta''}^{*})_{\text{in}} - (P_{\eta''}^{*})_{\text{out}} \Big) d\eta' d\eta'' \overset{\text{for Eq. 8}}{=} \frac{1}{\tau_r P_{\eta}^{**}} \Big((1-\bar{\xi})\eta - \int_0^{\eta} \int_0^{\eta'} (P_{\eta''}^{*})_{\text{out}} \, d\eta' d\eta'' \Big), \tag{9}$$

where $\bar{\xi}$ is the well-mixed mixture fraction calculated from the mass flow rates of the inlet streams. For example, consider a fuel stream with mass flow rate $\dot{m}_{\text{f}}$ and an oxidiser stream with $\dot{m}_{\text{ox}}$, then $\bar{\xi} = 1/(1 + \dot{m}_{\text{ox}}/\dot{m}_{\text{f}})$.

2.2 Solution strategy

The ISR approach for autoignition risk quantification starts with the calculation of the average non-reacting flow field using CFD. As discussed in [29], the modelling approach for the reference CFD simulation can vary given the availability of resources, but care must be taken for each specific application so that the underlying mixing field is well captured.

It is important to note that flame growth and stabilisation are not of particular interest from a risk assessment and rare event identification perspective. Consequently, flame effects to the mixing field do not need to be considered in the approach, similar to what was attempted in [31, 32]. In addition, perturbations to influential variables, such as fuel composition and temperature at the premixer inlet, do not affect the inert flow significantly but can alter autoignition behaviour; thus, non-reacting CFD can be reliably used to describe mixing and then coupled with an ISR for performing sensitivity analyses within a relatively wide range of conditions (concerning autoignition propensity) and training a surrogate model.

The ISR equations are then solved using an in-house code. Here the form of Eq. 8 is selected since the focus is on aeroderivative premixers with completely unmixed inlet streams. The evaluation of the core-averaged SDR via Eq. 9 requires knowledge of the mean residence time and the mixture fraction PDF. In this work, these quantities are extracted from a non-reacting CFD simulation, described in detail later. The core-averaged density and mixture fraction PDF are found using Eq. 3 for which some information of the CFD grid is required. At each CFD cell, P_{η} is modelled with a presumed β-function computed from the time-averaged mixture fraction and mixture fraction variance, which are readily available from the simulation. In the case of singularities, the β-function is replaced or complemented by δ-functions.

In Eq. 9, it is evident that the division with the core-averaged PDF can lead to numerical problems when the PDF tends to zero. To ensure that the SDR does not take unrealistically high values, the division with the PDF can be approximated as $1/P_{\eta}^{**} \approx P_{\eta}^{**}/(P_{\eta}^{**2} + \epsilon^2)$, where ϵ an absolute tolerance for the core-averaged PDF (here $\epsilon = 10^{-9}$). The double integration in Eq. 9 can also prove cumbersome and may result in negative values of the SDR due to machine precision errors when the PDF tends to zero [24]. The realisability problem could be solved using the methods of [39, 40] to find the double integrals numerically without limitations to the PDF shape. However, this might not prove necessary in a premixer system with completely unmixed streams. Assuming that the outlet PDF follows a narrow normal distribution in mixture fraction space around the well-mixed value, i.e., $(P_{\eta}^{*})_{\text{out}} \rightarrow \mathcal{N}(\bar{\xi}, \sigma_{\text{o}}^2)$, the double integral can be found analytically using:

$$\int_0^{\eta} \int_0^{\eta'} (P_{\eta''}^{*})_{\text{out}} \, d\eta' d\eta'' = \frac{1}{2} \Bigg((\eta - \bar{\xi}) \Big(1 + \text{erf}\big(\frac{\eta - \bar{\xi}}{\sqrt{2\sigma_{\text{o}}^2}} \big) \Big) + \sqrt{\frac{2\sigma_{\text{o}}^2}{\pi}} \exp\big(-\frac{(\eta - \bar{\xi})^2}{2\sigma_{\text{o}}^2} \big) \Bigg). \tag{10}$$

Equation 10 is used to calculate the double integral of the outlet mixture fraction PDF after finding an appropriate standard deviation matching the CFD simulation. Interestingly, in the limit of $\sigma_{\text{o}} \rightarrow 0$, i.e., perfect mixing at the outlet, it follows that $(P_{\eta}^{*})_{\text{out}} \rightarrow \delta(\eta - \bar{\xi})$, and its double integral is given by $(\eta - \bar{\xi})\mathcal{H}(\eta - \bar{\xi})$ where $\mathcal{H}$ the Heaviside function. As mentioned previously, the outlet PDF can also be numerically integrated if care is taken to locations of negligible probability [40]. Hence, there is no limitation in the configurations that can be represented.

For a scalar ϕ with a conditional mean Q_{ϕ}, the unconditional mean counterpart within the premixer core and at the outlet can then be found by:

$$\phi^{**} = \int_0^1 Q_{\phi} P_{\eta}^{**} \, d\eta; \quad \phi_{\text{out}} = \int_0^1 Q_{\phi} (P_{\eta}^{*})_{\text{out}} \, d\eta. \tag{11}$$

As far as the numerical setup of the ISR equations is concerned, mixture fraction space is discretised using 101 nodes clustered around the stoichiometric mixture fraction and sufficient resolution around the most-reactive mixture fraction [4], which will be described later. Pure air is imposed at $\eta = 0$, whereas the fuel composition is imposed at $\eta = 1$. The oxidiser, T_{ox}, and fuel temperature, T_f, are also imposed at the boundaries $\eta = 0$ and $\eta = 1$, respectively. The pressure is assumed constant and equal to the nominal operating pressure of the premixer. The system is assumed adiabatic; therefore, the conditional enthalpy remains constant throughout computations and the conditional temperature may be identified via a reverse calculation (here with an absolute tolerance of 10^{-8}). All simulations are initialised from "pure mixing" solutions using the same boundary conditions. As will be detailed later, the fuel composition, T_{ox} and T_f and their uncertainty are studied in detail in this paper since they are crucial for autoignition.

An operator splitting technique is then implemented for the solution of the ISR equations, which are marched in time until convergence is reached. First, the diffusion term of Eq. 8 is computed using a second-order accurate numerical scheme and the VODPK solver [41], followed by the integration of the chemistry employing the chemical mechanism by Jella et al. [1] and first-order moment closure [24]. The effect of the operator splitting between diffusion and chemistry has been assessed at steady-state with an Amplitude Mapping Closure (AMC) model [42] for the conditional SDR profile. The results were then compared with the method of lines finding negligible differences for temperature, major species and radicals for pseudo-time steps below 2 μs (e.g., see [43] for a similar assessment applied to the elliptic CMC equation). A constant time step of 1 μs is used here.

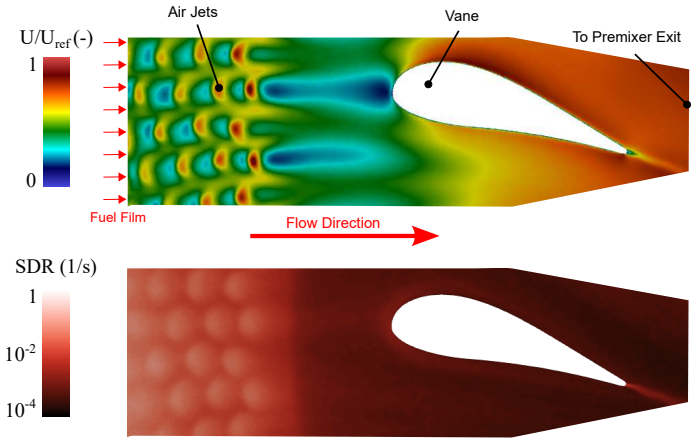

FIGURE 1: NORMALISED MEAN VELOCITY MANGNITUDE FIELD (TOP) AND MEAN SCALAR DISSIPATION RATE IN A SECTION OF THE INVESTIGATED PREMIXER (BOTTOM).

3. INVESTIGATED PREMIXER AND CFD ANALYSIS

An experimental premixer is investigated here to demonstrate the ISR stochastic analysis frameworks. The same premixer was studied previously by Jella et al. using reacting CFD [1]. Furthermore, Gkantonas et al. [32] successfully employed ISR theory to estimate autoignition propensity in this premixer, so it was preferred here as a benchmark case. The premixer was designed to have a characteristic residence time approximately six times shorter than the worst case autoignition delay of typical natural gas and features multiple jets injecting pure air into a cross stream of gaseous fuel in the form of a film [1]. The distributed injection of air and fuel results in a range of residence times that significantly damps Intermediate Frequency Dynamics for a wide range of operating conditions [44].

A representation of the mean flow and mixing fields obtained with non-reacting LES is shown in Fig. 1. The Favre-filtered continuity and momentum equations, as well as transport equations for the mixture fraction, $\widetilde{\xi}$, and its sub-grid scale variance, $\widetilde{\xi''^2}$, were solved using the Star-CCM+ CFD software. The Wall-Adaptive Large Eddy Simulation (WALE) model of Nicoud and Ducros [45] was used to model sub-grid stresses. The filtered scalar dissipation rate, $\widetilde{N}$, used in the sub-grid scale variance transport equation, was computed considering both the resolved and sub-grid scale contributions [46, 47] as in $\widetilde{N} = D\vec{\nabla}\widetilde{\xi}\cdot\vec{\nabla}\widetilde{\xi} + C_N\widetilde{\xi''^2}\mu_{\text{sgs}}/(2\rho\Delta^2)$, where $C_N = 42$ [48, 49], μ_{sgs} the sub-grid scale viscosity and Δ the filter width estimated as the cube root of the LES cell volume. The molecular diffusivity was calculated from the kinematic viscosity of the mixture using a constant Schmidt number ($Sc = 0.7$). A bounded central differencing scheme was employed for the convective terms in the momentum equation while the diffusion terms were discretised using pure central differencing. Second-order upwinding was used for all scalars. The temporal terms were discretised using an implicit second-order backward differencing scheme, and a time-step restricting the CFL number to less than 0.5 was chosen. The mesh cell size in the premixer was 0.2 mm or smaller.

The CFD simulation was set at representative full load conditions. These conditions were chosen as the combination of preheat, pressure and stoichiometry represents a highly reactive operating scenario. In addition, the fuel mixture composition is also of critical importance. In service, the engine is operated with natural gas. However, a gaseous blend of highly reactive dimethyl ether (DME) fuel and less reactive methane (CH_4) is used in this experimental premixer to increase the frequency of autoignition events [1]. As discussed in [1], gaseous DME is used to increase the reactivity of methane and thus model the effect that higher hydrocarbons may have on the fuel autoignition propensity. DME-blended methane is then employed to test the robustness of high-pressure premixers to autoignition. The CFD simulation considered a fuel mixture of pure CH_4 with 40% (v/v) DME. As explained in Section 4, the fuel composition, as well as the temperatures of the air and fuel streams, are modified in the ISR computations, but considering the same underlying mixing field. As the deviations are deemed small enough to cause little differences in velocity and density, the changes in the mixture fraction distribution are negligible.

A detailed CFD analysis on this premixer has already been provided by Jella et al. [1], so only a brief summary is provided here. Figure 1 shows the normalised mean velocity magnitude and mean scalar dissipation rate (SDR) fields in a section of the premixer, as computed from the non-reacting simulation. The presence of the air jets can be inferred by the red "spots" in the mean velocity field in the upstream region, indicating high velocity. Each red spot is also associated with a wake on the lee side that affects the local residence time and mixing rate. The flow decelerates between the last row of air jets and the guide vane, and is then quickly accelerated on its way to the vane's trailing edge and towards the premixer exit. Until the flow reaches the premixer exit, the mixing intensity is low and the mixture fraction has attained closely the well-mixed value as can be indicated by the overall very low SDR values in the downstream region of Fig. 1. Most of the mixing occurs near the fuel injection region where the SDR is very high (not shown). Towards the last rows of air jets, the scalar dissipation rate obtains moderate values but can still span several orders in magnitude depending on the location relative to the air jets, until a significant decay is observed soon after the last row or air jets.

Information regarding the mixing field can also be obtained through the core-averaged mixture fraction PDF, P^{**}_{η}, which is also directly used in the ISR computations. Figure 2 shows the profile of P^{**}_{η} as a function of η, i.e., the sample space variable for the mixture fraction, up to a reference mixture fraction, η_0. Two peaks are evident in the PDF profile, one at $\eta = 0$ corresponding to the air stream and another at the well-mixed mixture fraction, $\bar{\xi}$. In reality, the PDF profile is tri-modal since another peak exists at $\eta = 1$ corresponding to the fuel stream (not shown). The local distribution and the width around $\bar{\xi}$ are a measure of the unmixedness within the premixer. For the same residence time, the higher the PDF at a particular mixture fraction, the lower the local value of the conditional SDR, as inferred by Eq. 9. At the same time, the PDF indicates the extent at which the stoichiometric, ξ_{st}, and the most reactive mixture fractions ξ_{mr} (as defined by Mastorakos [4]) are present in the premixer at both the large and small scales.

The most reactive mixture fraction corresponds to the loca-

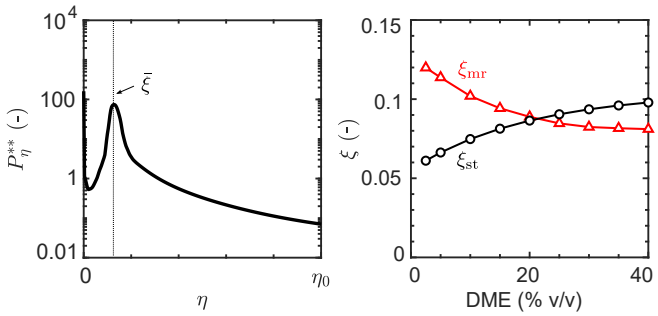

FIGURE 2: CORE-AVERAGED MIXTURE FRACTION PDF WITH WELL-MIXED MIXTURE FRACTION INDICATED (LEFT) AND DEPENDENCE OF STOICHIOMETRIC AND MOST REACTIVE MIXTURE FRACTION TO AMOUNT OF DME IN THE FUEL FOR THE REFERENCE TEMPERATURES (RIGHT).

tion of the first autoignition kernel in mixture fraction space in the absence of hydrodynamic stretch. The difference in temperature between the fuel and oxidiser streams inevitably results in variable autoignition delay times for each mixture fraction, with ξ_{mr} having the most favourable conditions for autoignition, at least when micromixing effects are not present. Figure 2 shows the dependency of ξ_{st} and ξ_{mr} with increasing level of DME. The premixer's target equivalence ratio is overall fuel-lean with $\bar{\xi}$ being significantly smaller than ξ_{st} and ξ_{mr} for all conditions. It is also evident that up to about 20% (v/v) DME in the fuel, the first autoignition kernel is more likely to occur in fuel-rich zones, whereas for higher DME levels, autoignition is more likely in fuel-lean zones. With different operating conditions, ξ_{st} and ξ_{mr} differ but so is the probability of finding these mixture fractions in the premixer. These observations are important for the remainder of the discussion since they can help explain some of the trends observed in the stochastic analysis.

4. STOCHASTIC ANALYSIS FRAMEWORK

Once the mixing field from the non-reacting LES simulation is averaged, the ISR approach described in Section 2 can then be applied. An ISR network (ISRN) approach can be also applied on the same LES simulation, and results obtained by ISRN in terms of autoignition propensity and its sensitivity to operating conditions have been presented by Gkantonas et al. [32]. However, the ISR approach guarantees lower computational costs than the ISRN one while maintaining acceptable accuracy, as a close agreement in terms of premixer autoignition behaviour between the two approaches was observed. As this study focuses only on the occurrence, or the absence, of autoignition inside the premixer, which can be captured by a single ISR, the latter is employed.

The boundary conditions are considered fixed for each ISR simulation. In reality, uncertainties and fluctuations affect the nominal values of the boundary conditions, introducing stochasticity in the output quantities of the premixer. The effect of the random variability of input parameters on the premixer behaviour must be predicted and quantified via a stochastic analysis. Figure 3 depicts the general framework of the stochastic analysis adopted in this work. Three random input quantities to the premixer were considered, namely the fuel temperature (T_f), the air temperature (T_{ox}), and the amount of DME in the fuel mixture consisting primarily of methane. A space-filling design was generated over the three-dimensional parameter space via the Latin Hypercube Sampling (LHS) method [50]. For each sampled combination, numerical simulations were performed with the ISR approach. A surrogate model (also called meta-model or response surface) was trained on selected autoignition (AI) metrics obtained as output from the ISR simulations. A brute-force Monte Carlo sampling of the probability density functions (PDFs) of the input parameters was performed and the samples were fed to the surrogate model to obtain the characterisation of the distributions of the selected AI metrics. The AI metrics are selected at the premixer exit and correspond to the mass-averaged temperature, T^*_{out}, and the conditional temperature at stoichiometry, $\langle T|\eta_{st}\rangle_{out}$ (η_{st} being the sample space variable of the mixture fraction at stoichiometry, ξ_{st}). They allow to determine if an autoignition kernel formation event has occurred in the premixer, whereas their probability density function, obtained via Monte Carlo sampling, provides the frequency of autoignition and hence a quantification of the autoignition risk.

The methodology described above was slightly modified by the inclusion, prior to the surrogate training step, of a classification method through which the 3-dimensional parameter space was clustered in two different subspaces. As a consequence, two separate surrogate models were trained on the corresponding subspaces and achieved higher fitting accuracy than those obtained by only one surrogate model trained on the whole parameter space. Further details are provided in the following section.

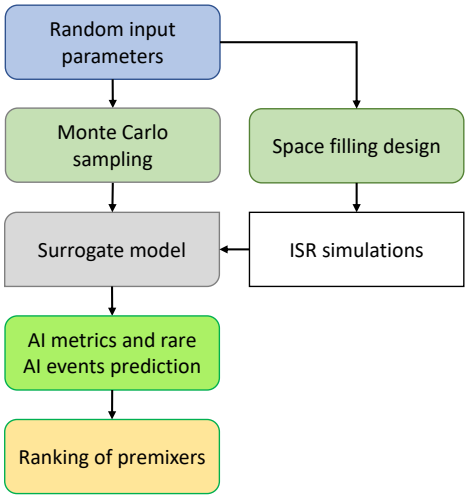

FIGURE 3: METHODOLOGY SCHEME.

5. RESULTS AND DISCUSSION

An event can be classified as rare if the frequency of its occurrence is low, or when the overall observational cost is so large that a specific procedure is required to induce it [51]. Although there is no probability level that universally defines a rare event, if we consider a random variable described by a normal distribution, we can say that rare variable outcomes are located at the PDF tails,

which require special focus. The aim of this work is to explore the nature of the tail of the PDF of quantities that can be related to the occurrence of high-temperature autoignition in a premixer, given a PDF of three input parameters, i.e. T_f, T_{ox}, and %DME in the fuel mixture. Normal distributions were considered for the three parameters, with variable means, representing different operating conditions, and fixed standard deviations, equal to 5 K, 10 K and 2%, for T_f, T_{ox}, and %DME, respectively. For the space-filling design, the ranges of variability of the parameters were set to include the different mean values and their ±5-6σ uncertainty. A total of 500 different combinations were sampled from the parameter space via LHS, and 500 ISR simulations were performed for each input combination. The simulations took about 5 hours to run concurrently over 20 processors. Figures 4 and 5 show the values of T^*_{out} and $\langle T|\eta_{\text{st}}\rangle_{\text{out}}$ obtained by each ISR simulation. In the figures, T_{ox}, T^*_{out} and $\langle T|\eta_{\text{st}}\rangle_{\text{out}}$ are normalised by the reference value of T_{ox}, i.e. at the representative full load state, $T_{ox,\text{ref}}$, whereas T_f is normalised by the reference value of T_f, $T_{f,\text{ref}}$. It can be seen that the two AI metrics correlate with each other since high values of T^*_{out} correspond to high values of $\langle T|\eta_{\text{st}}\rangle_{\text{out}}$. A more pronounced discontinuity can be noticed in the values of the conditional temperature at stoichiometry at the exit of the premixer, $\langle T|\eta_{\text{st}}\rangle_{\text{out}}$. Since T^*_{out} is a mass-averaged temperature (see also Eq. 11), its values are lower than the corresponding ones of $\langle T|\eta_{\text{st}}\rangle_{\text{out}}$. Hereafter, the results of the methodology described in Section 4 will be shown only for one of the two AI metrics, namely T^*_{out}, as the two quantities strongly correlate with each other and the results obtained for $\langle T|\eta_{\text{st}}\rangle_{\text{out}}$ would lead to the same discussions and conclusions. The normalised values of $T_{ox}/T_{ox,\text{ref}}$, $T_f/T_{f,\text{ref}}$ and $T^*_{\text{out}}/T_{ox,\text{ref}}$ will be reported.

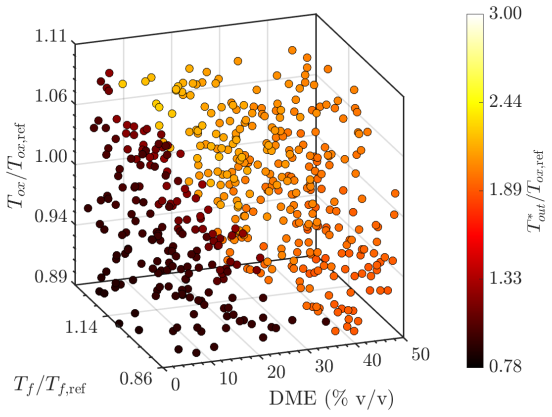

FIGURE 4: $T^*_{\text{out}}/T_{ox,\text{ref}}$ OBTAINED BY THE 500 ISR SIMULATIONS.

The training of the surrogate model was attempted for T^*_{out} over the whole parameter space. The accuracy of the surrogate was evaluated during training by 5-fold cross validation. After training, the surrogate fitting errors, i.e., the difference between the values of T^*_{out} provided by the 500 ISR simulation and the corresponding values obtained by the surrogate model, were evaluated. Several surrogate models, such as quadratic and rational-quadratic polynomials, Gaussian Processes (GPs) and support-vector machines (SVMs), were trained in MATLAB on all the 500 T^*_{out} values but none provided acceptable fitting errors

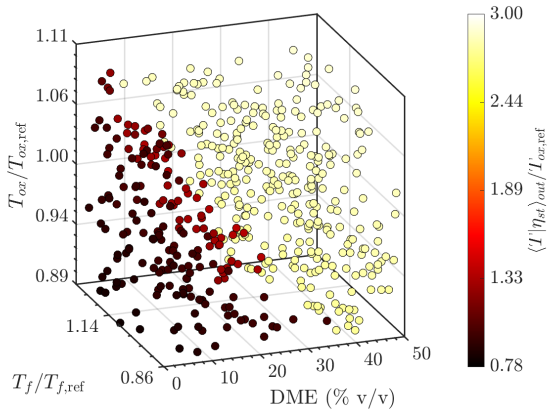

FIGURE 5: $\langle T|\eta_{\text{st}}\rangle_{\text{out}}/T_{ox,\text{ref}}$ OBTAINED BY THE 500 ISR SIMULATIONS.

(not shown here). It can be seen in Fig. 4 that a sharp discontinuity exists in the set of $T^*_{\text{out}}/T_{ox,\text{ref}}$ values as there are no values between about 1.33 and 1.89. This can affect the training of response surface and lead to large fitting errors. Thus, a normalised threshold value $(T^*_{\text{out}}/T_{ox,\text{ref}})_{\text{tr}} = 1.67$ was chosen to distinguish two distinct regions: the subspace of input parameter values at which high-temperature autoignition does not occur inside the premixer, corresponding to values of $T^*_{\text{out}}/T_{ox,\text{ref}} \leq 1.67$, and the subspace where autoignition brings the normalised mass-averaged temperature at the premixer exit above 1.67, namely $T^*_{\text{out}}/T_{ox,\text{ref}} > 1.67$. The different behaviours are mostly correlated to the variability of T_{ox} and %DME, while the occurrence of autoignition seems to be less sensitive to T_f. A classification algorithm, or classifier, can be trained on the ISR responses to automatically distinguish between no-ignition and autoignition regimes. For each regime, a separate response surface can be constructed to map the stochastic input parameters to the AI metrics. The methodology scheme of Fig. 3 was then modified to include the classification step prior to the training of the surrogate models. In the updated scheme, shown in Fig. 6, the ISR responses are used to train the classifier and the surrogate models. The input parameter combinations sampled via Monte Carlo are provided to the classifier first, which assigns each combination to either the no-ignition or the autoignition regime. Based on the assigned regime, the corresponding surrogate model yields the output quantity. Eventually, the characterisation of the distributions of the selected AI metrics, and thus a quantification of autoignition risk, are obtained.

Several classifiers were trained and compared based on their accuracy, which was evaluated via 5-fold cross-validation. The Classification Learner module in MATLAB was used for this task. Logistic Regression provided the highest accuracy (99.2%) in classifying the no-ignition vs autoignition regimes, as can be seen in Fig. 7, which shows the scatter of the input $T_{ox}/T_{ox,\text{ref}}$ and %DME values and the separation between the no-ignition region, marked by blue dots, and the autoignition one, marked by red dots. The crosses indicates the combinations of input values that were wrongly assigned to a certain regime.

After the classification step, two different response surfaces

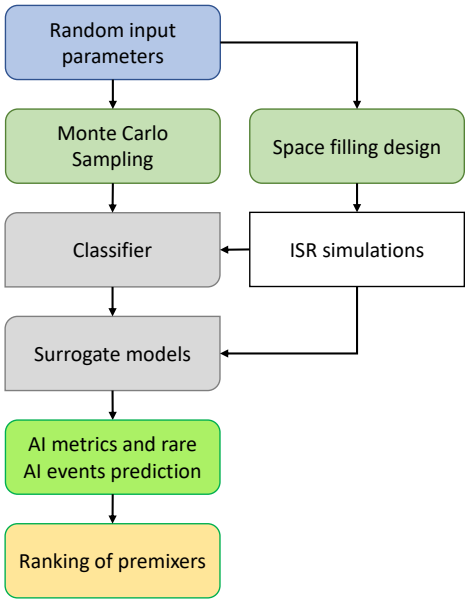

FIGURE 6: METHODOLOGY SCHEME MODIFIED BY THE PRESENCE OF A CLASSIFICATION STEP BEFORE THE SURROGATE MODEL TRAINING.

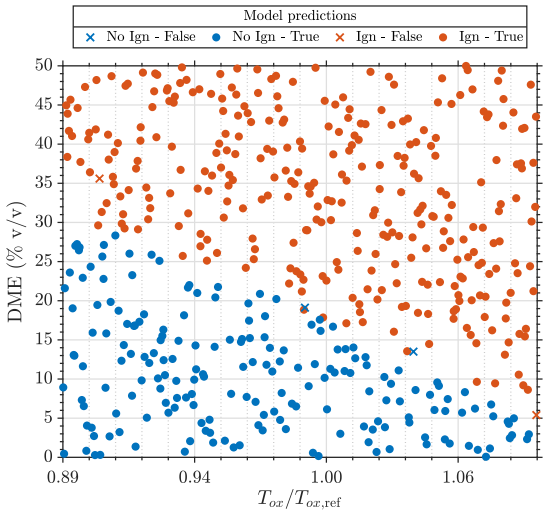

FIGURE 7: CLASSIFICATION OF T^*_{out}. TWO CLUSTERS ARE DISTINGUISHED BY THE CLASSIFIER: THE "NO IGNITION" REGION (BLUE DOTS) AND THE "AUTOIGNITION" REGION (RED DOTS). THE CROSSES INDICATE POINTS THAT ARE WRONGLY ASSIGNED BY THE CLASSIFIER.

were trained for low T^*_{out} values ($T^*_{\mathrm{out}}/T_{ox,\mathrm{ref}} \leq 1.67$) and high T^*_{out} values ($T^*_{\mathrm{out}}/T_{ox,\mathrm{ref}} > 1.67$). Figure 8 shows the parity plot comparing the low $T^*_{\mathrm{out}}/T_{ox,\mathrm{ref}}$ values obtained by the ISR simulations and those obtained by a Gaussian Process (GP) with Matérn 5/2 kernel (whose mathematical description and details can be found in [52]) trained in the no-ignition region of the parameter space. Figure 8 also reports the histogram of the surrogate fitting errors, defined as $\delta_T = |T^*_{out,\mathrm{GP}} - T^*_{out,\mathrm{ISR}}|$, where $T^*_{out,\mathrm{GP}}$ and $T^*_{out,\mathrm{ISR}}$ are the values of the mass-averaged exit temperature obtained by the GP and the ISR, respectively. The low-order model is able to predict the low T^*_{out} values with acceptable accuracy as the maximum fitting error is lower than 60 K (corresponding to a relative error lower than 6%). Similarly, Figure 9 shows the parity plot of the high $T^*_{\mathrm{out}}/T_{ox,\mathrm{ref}}$ values obtained by the ISR simulations and another GP with Matérn 5/2 kernel trained in the autoignition region of the parameter space. Figure 9 also reports the histogram of the GP fitting errors δ_T previously defined. The low-order model fits the high T^*_{out} values with excellent accuracy as the maximum fitting error is lower than 1 K. The training of the two GPs was performed in less than one minute on a 4-core laptop. The higher accuracy of the GP for high T^*_{out} can be explained by two considerations. First, the number of training points is higher in the autoignition region of the parameter space since about 62% of the sampled input combinations determine autoignition in the ISR simulations. A lower number of samples may affect the accuracy of the response surface fitting. Second, the no-ignition region may actually contain ISR simulations where a cool flame exists, characteristic of DME-air combustion (e.g., see [53] for a recent review on the topic). This may be defined as low-temperature autoignition. By looking at the parity plot of Fig. 8, sparse data around 1.11 can be noticed, possibly indicating a discontinuity related to the occurrence of low-temperature autoignition. A third subspace may be identified by considering $T^*_{\mathrm{out}}/T_{ox,\mathrm{ref}}$ lower than 1.67 but higher than 1.11, where another surrogate model may be trained with lower fitting errors. An unsupervised classifier can also be used to distinguish the no-ignition and ignition regions without the need to specify a temperature threshold. Depending on the number of training points, an unsupervised classifier might have higher accuracy than the classifier used in this work. It might also distinguish the no-ignition region from the low-temperature autoignition one, where cool flames, characteristic of DME-air combustion, occur. These are open questions that will be addressed in future studies.

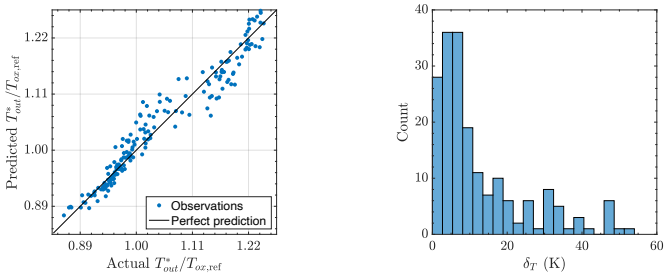

FIGURE 8: PARITY PLOT OF NORMALISED MASS-AVERAGED EXIT TEMPERATURES $T^*_{\mathrm{out}}/T_{ox,\mathrm{ref}} \leq 1.67$ OBTAINED BY THE ISR SIMULATIONS AND THE SURROGATE MODEL (LEFT) AND HISTOGRAM OF THE FITTING ERRORS OF THE SURROGATE MODEL (RIGHT).

The capability of the trained Gaussian Processes to predict a PDF of T^*_{out} was assessed by considering only one random input quantity, which was described by a hypothetical normal distribution with normalised mean $\mu = 0.99$ and normalised standard deviation $\sigma = 0.01$, i.e., $T_{ox}/T_{ox,\mathrm{ref}} = \mathcal{N}(0.99, 0.01)$. Additional 45 ISR simulations were performed at fixed %DME = 40 and normalised $T_f/T_{f,\mathrm{ref}} = 0.92$, while $T_{ox}/T_{ox,\mathrm{ref}}$ was instead varied

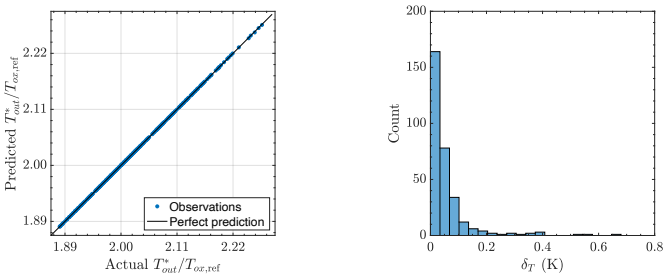

FIGURE 9: PARITY PLOT OF NORMALISED MASS-AVERAGED EXIT TEMPERATURES $T^*_{out}/T_{ox,ref} > 1.67$ OBTAINED BY THE ISR SIMULATIONS AND THE SURROGATE MODEL (LEFT) AND HISTOGRAM OF THE FITTING ERRORS OF THE SURROGATE MODEL (RIGHT).

from 0.93 to 1.05, and provided 45 $T^*_{\text{out}}/T_{ox,\text{ref}}$ values above 1.67. By knowing the correspondence between T_{ox} and T^*_{out} values, a PDF of T^*_{out} can be established a priori. The Gaussian Process trained for high T^*_{out} must be able to replicate this known PDF. The latter was compared to the one obtained from 10^8 realisations of T^*_{out} provided by the Gaussian Process queried by as many random samples from the normal distribution of T_{ox}. The 10^8 realisations of T^*_{out} were computed in less than 4 hours on a 12-core processor. Excellent agreement was found between the known PDF of T^*_{out} and the one computed by the GP, as shown in Fig. 10, even for very low PDF values, of the order of 10^{-7}. In Fig. 10, the PDF values are related to the non-normalised values of T^*_{out}, although the normalised values of $T^*_{\text{out}}/T_{ox,\text{ref}}$ are reported. This result confirms the accuracy of the GP, even for additional data points that were not used for the training of the GP itself, and validates the use of a response surface for fast estimation of an autoignition metric.

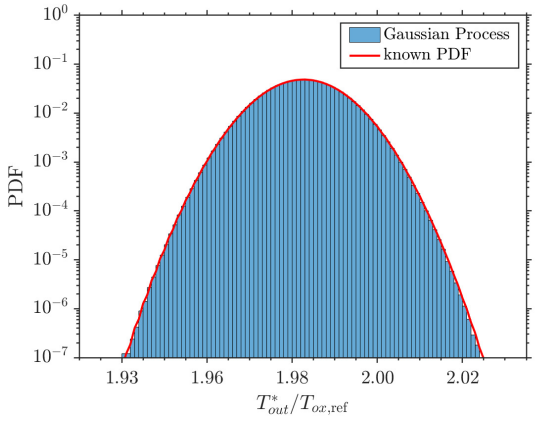

FIGURE 10: PDF (IN LOGARITHMIC SCALE) OF T^*_{out} OBTAINED BY THE TRAINED GAUSSIAN PROCESS WHEN PROPAGATING THE UNCERTAINTY OF ONLY ONE INPUT QUANTITY, T_{ox}, CHARACTERISED BY A DISTRIBUTION $T_{ox}/T_{ox,\text{ref}} = \mathcal{N}(0.99, 0.01)$.

At the Monte Carlo sampling stage, normal distributions are assumed for T_f, T_{ox}, and %DME, having (non-normalised) standard deviations $\sigma_{T_f} = 5$ K, $\sigma_{T_{ox}} = 10$ K, and $\sigma_{\%\text{DME}} = 2$, respectively. First, the following mean values are considered for the input distributions: $\mu_{T_f} = 0.92\,T_{f,\text{ref}}$, $\mu_{T_{ox}} = 0.99\,T_{ox,\text{ref}}$, and $\mu_{\%\text{DME}} = 20$. A total of 10^7 random samples of the Gaussian PDFs were provided to the classifier and assigned to the corresponding subspaces where T^*_{out} was computed by the related surrogate model. Figure 11 shows the obtained scatter of $T^*_{\text{out}}/T_{ox,\text{ref}}$ values, along with the output of the ISR simulations. The ISR values of $T^*_{\text{out}}/T_{ox,\text{ref}}$ are indicated by filled circles, whereas the 10^7 surrogate realisations of $T^*_{\text{out}}/T_{ox,\text{ref}}$ are marked by empty circles. A PDF of the non-normalised T^*_{out} values was then obtained and is also shown in Fig. 11. The probability of $T^*_{\text{out}} > T^*_{\text{out,tr}}$, with $T^*_{\text{out,tr}} = 1.67\,T_{ox,\text{ref}}$, can be seen as the autoignition probability in the premixer at the considered nominal (mean) values of the input quantities and is given by $P_{AI} = \int_{T^*_{\text{out,tr}}}^{\infty} P(T^*_{\text{out}})dT^*_{\text{out}}$. At these conditions, the probability that autoignition would occur in the premixer is about 54.6%.

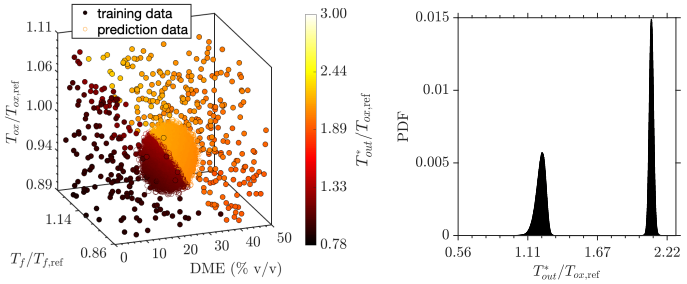

FIGURE 11: (LEFT) $T^*_{\text{out}}/T_{ox,\text{ref}}$ OBTAINED BY THE 500 ISR RUNS (FILLED CIRCLES) AND THE 10^7 REALISATIONS OF THE SURROGATE MODELS (OPEN CIRCLES). (RIGHT) PDF OF T^*_{out} COMPUTED BY THE SURROGATE MODELS.

Different mean values of T_f, T_{ox}, and %DME can be considered, while keeping constant their standard deviations. Since the fuel temperature appears to have the lowest influence on the onset of autoignition in the premixer, the autoignition risk was quantified at different mean value pairs of T_{ox} and %DME, while keeping $T_f/T_{f,\text{ref}} = 0.92$ fixed. Figure 12 shows the probability distributions of T^*_{out} obtained at normalised $\mu_{T_{ox}}/T_{ox,\text{ref}} \equiv \overline{T}_{ox}/T_{ox,\text{ref}} = 0.96$, 0.99, 1.02, and $\mu_{\%\text{DME}} = 0$, 20, 40. When $\mu_{\%\text{DME}} = 0$, the volumetric amount of DME in the fuel mixture cannot be negative, hence a half-normal PDF of %DME was considered for the positive values of %DME. Once again, 10^7 random combinations were sampled for each case. It can been seen from Fig. 12 that autoignition never occurs for the lowest amounts of DME in the fuel mixture as increasing the air temperature does not change the premixer behaviour. When the mean volumetric amount of DME is equal to 20%, autoignition occurs 5% of the time at $\mu_{T_{ox}}/T_{ox,\text{ref}} = 0.96$, and increasing the air temperature determines a higher probability of autoignition, up to 97% at $\mu_{T_{ox}}/T_{ox,\text{ref}} = 1.02$. Finally, when the mean volumetric amount of DME is 40%, autoignition occurs at all the considered mean air temperatures.

In order to capture rare autoignition events, the analysis described above was repeated for another set of mean values, i.e., $\mu_{T_f}/T_{f,\text{ref}} = 0.95$, $\mu_{T_{ox}}/T_{ox,\text{ref}} = 1.03$, and $\mu_{\%\text{DME}} = 3$. Since computing a probability of order 10^{-6} with 90% accuracy requires around 10^8 realisations [51], as many random samples have been taken and fed to the classifier and the surrogate models. Sam-

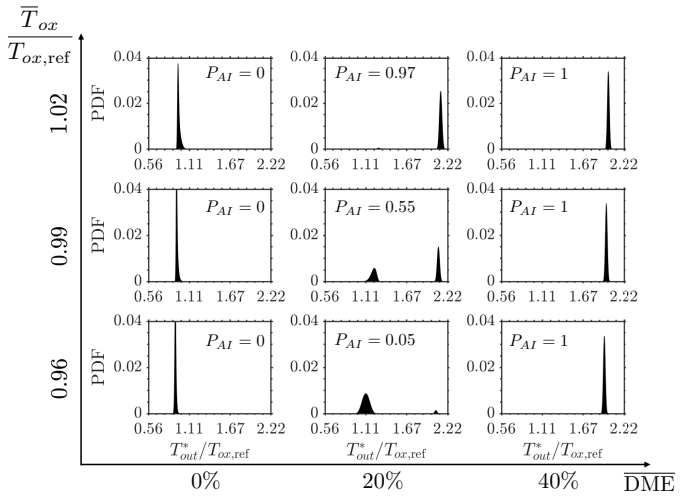

FIGURE 12: PDFS OF T^*_{out} AT DIFFERENT MEAN VALUES OF T_{ox} AND %DME AND CORRESPONDING AUTOIGNITION PROBABILITIES P_{AI}.

ples with negative values of %DME were disregarded during the process. The resulting values of $T^*_{\mathrm{out}}/T_{ox,\mathrm{ref}}$ are shown in Fig. 13, which also illustrates the position of the sampled region in the parameter space. The cloud of sampled points barely crosses the autoignition subspace, indicating autoignition may occur in the premixer at these conditions. The resulting PDF of T^*_{out} is also shown in Fig. 13 (note that the vertical axis is logarithmic) and confirms the occurrence of rare autoignition events bringing $T^*_{\mathrm{out}}//T_{ox,\mathrm{ref}}$ up to around 2.22. At these conditions, the probability that autoignition would occur in the premixer was calculated as previously described and is equal to $P_{AI} = 2.8 \cdot 10^{-6}$.

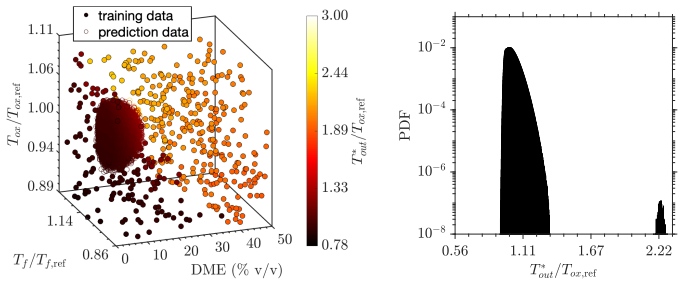

FIGURE 13: (LEFT) $T^*_{\mathrm{out}}/T_{ox,\mathrm{ref}}$ OBTAINED BY THE 500 ISR RUNS (FILLED CIRCLES) AND THE 10^8 REALISATIONS OF THE SURROGATE MODELS (OPEN CIRCLES). (RIGHT) PDF (IN LOGARITHMIC SCALE) OF T^*_{out} COMPUTED BY THE SURROGATE MODELS.

6. SUMMARY AND CONCLUSIONS

A novel approach using Incompletely Stirred Reactor (ISR) post-processing on a non-reactive CFD solution and surrogate modelling for stochastic estimation of non-premixed autoignition in a aeroderivative premixer has been presented. The variability of three influential input parameters, i.e., fuel temperature, air temperature, and volume fraction of dimethyl ether (DME) in the fuel mixture, was propagated to estimate the distributions of physical quantities labelled as autoignition metrics, as they can indicate the occurrence of high-temperature autoignition inside the premixer. In this work, the mass-averaged temperature at the premixer exit was chosen as the target autoignition metric.

A total of 500 ISR simulations of the premixer were first performed at input parameter combinations sampled via a space-filling design. The obtained estimations of the mass-averaged temperature at the premixer exit revealed the presence of two distinct regions of the 3-dimensional parameter space, which hindered the training of a single surrogate model for the chosen autoignition metric. Thus, a classification step was introduced before the response surface training to distinguish the no-ignition and autoignition regions. The classifier was trained on the already performed 500 ISR simulations. On each sub-region of the parameter space identified by the classifier, an accurate surrogate model was then trained for the autoignition metric on the same ISR simulations. The probability distribution of the mass-averaged exit temperature was then computed by propagating the variability of the input parameters via Monte-Carlo sampling. The classifier assigned each random sample to the correct subspace, where the corresponding surrogate model mapped the input parameters to the autoignition metric. The autoignition probability was then estimated at several nominal values of the input quantities by integrating the obtained probability density functions of the mass-averaged exit temperature.

In order to obtain a reliable estimate of probabilities of rare events, such as autoignition in an aeroderivative premixer, a large number of realisations is necessary. For Monte Carlo methods, computing a probability of order 10^{-6} with 90% accuracy requires around 10^8 realisations. Intense research focused on mitigating this issue, leading to variance reduction methods for unbiased probability estimators. The issue is alleviated here by employing response surfaces that can provide 10^8 realisations at much reduced computational costs without limited loss of accuracy. Moreover, the training of accurate response surfaces may require a significant number of CFD simulations, up to a point where using response surfaces does not reduce any computational effort. This risk is mitigated by using an ISR approach which combines detailed chemistry with average flow and mixing fields obtained from one inert CFD simulation, thus keeping the computational cost at the lowest.

In this methodology, the accuracy of the autoignition risk quantification is strongly related to the efficiency of the classification method. The frontier that separates the no ignition and the autoignition regions must be predicted by the classifier correctly. Other classification algorithms, in a supervised or unsupervised fashion, can be employed to achieve higher accuracy. Moreover, instead of single ISR runs, simulations employing a network of ISRs, i.e., the Incompletely Stirred Reactor Network (ISRN) approach, can be leveraged to improve the characterisation of the border between the subspaces with a moderate computational penalty. The accuracy of a classifier, trained on both ISR and ISRN simulations, will benefit from the enhanced characterisation of the frontier manifold. Nonetheless, the methodology presented in this work has shown its capability to quantify the autoignition risk in an efficient and computationally feasible way. Small fluctuations of input parameters can cause significant

changes in the premixer output response, and simple physics-based tools that combine chemical reaction and mixing effects, such as the ISR approach, can be reliably used to study the premixer robustness to autoignition risk. Autoignition is expected to become more important in the future with a transition from conventional to next-generation fuels. Hence, it is very important to characterise the input uncertainties (e.g., in terms of a mean and a variance) and to be aware of the tails of the distributions (e.g., at ±6 standard deviations), so that premixer systems can be evaluated at these remote (typically off-design) conditions. Based on the autoignition risk, different premixers can be ranked, and the best premixer design and operating conditions can be selected for its intended use. The use of this joint ISR(N)-classifier-surrogate approach for premixer design optimisation for rare autoignition events will be the focus of future work.

PERMISSION FOR USE

ACKNOWLEDGEMENTS

The work at Cambridge was supported by Siemens Energy, whose financial support is acknowledged.

REFERENCES

[1] Jella, S., Bourque, G., Gauthier, P., Versailles, P., Bergthorson, J., Park, J.-W., Lu, T., Panigrahy, S. and Curran, H. "Analysis of Auto-Ignition Chemistry in Aeroderivative Premixers at Engine Conditions." *Journal of Engineering for Gas Turbines and Power* Vol. 143, No. 11 (2021): p. 111024. DOI 10.1115/1.4051460.

[2] Mastorakos, E., Baritaud, T.A. and Poinsot, T.J. "Numerical simulations of autoignition in turbulent mixing flows." *Combustion and Flame* Vol. 109, No. 1 (1997): pp. 198–223. DOI 10.1016/S0010-2180(96)00149-6.

[3] Markides, C.N. and Mastorakos, E. "An experimental study of hydrogen autoignition in a turbulent co-flow of heated air." *Proceedings of the Combustion Institute* Vol. 30, No. 1 (2005): pp. 883–891. DOI 10.1016/j.proci.2004.08.024.

[4] Mastorakos, E. "Ignition of turbulent non-premixed flames." *Progress in Energy and Combustion Science* Vol. 35, No. 1 (2009): pp. 57–97. DOI 10.1016/j.pecs.2008.07.002.

[5] Xiouris, C., Ye, T., Jayachandran, J. and Egolfopoulos, F.N. "Laminar flame speeds under engine-relevant conditions: Uncertainty quantification and minimization in spherically expanding flame experiments." *Combustion and Flame* Vol. 163 (2016): pp. 270–283. DOI 10.1016/j.combustflame.2015.10.003.

[6] Zhang, Y., Jeanson, M., Mével, R.., Chen, Z. and Chaumeix, N. "Tailored mixture properties for accurate laminar flame speed measurement from spherically expanding flames: Application to H2/O2/N2/He mixtures." *Combustion and Flame* Vol. 231 (2021): p. 111487. DOI 10.1016/j.combustflame.2021.111487.

[7] Prager, J., Najm, H.N., Sargsyan, K., Safta, C. and Pitz, W.J. "Uncertainty quantification of reaction mechanisms accounting for correlations introduced by rate rules and fitted Arrhenius parameters." *Combustion and Flame* Vol. 160, No. 9 (2013): pp. 1583–1593. DOI 10.1016/j.combustflame.2013.01.008.

[8] Ji, W., Wang, J., Zahm, O., Marzouk, Y.M., Yang, B., Ren, Z. and Law, C.K. "Shared low-dimensional subspaces for propagating kinetic uncertainty to multiple outputs." *Combustion and Flame* Vol. 190 (2018): pp. 146–157. DOI 10.1016/j.combustflame.2017.11.021.

[9] Lipardi, A.C.A., Versailles, P., Watson, G.M.G., Bourque, G. and Bergthorson, J.M. "Experimental and numerical study on NOx formation in CH4–air mixtures diluted with exhaust gas components." *Combustion and Flame* Vol. 179 (2017): pp. 325 – 337. DOI 10.1016/j.combustflame.2017.02.009.

[10] Yousefian, S., Bourque, G. and Monaghan, R.F.D. "Uncertainty Quantification of NOx and CO Emissions in a Swirl-Stabilized Burner." *Journal of Engineering for Gas Turbines and Power* Vol. 141, No. 10. DOI 10.1115/1.4044204.

[11] Iavarone, S., Bertolino, A., Cafiero, M. and Parente, A. "Combined effect of experimental and kinetic uncertainties on NO predictions in low-pressure premixed laminar H2/CH4/CO-air and H2/CH4/CO/C6H6-air flames." *Fuel* [under review].

[12] Oh, M.-S. and Berger, J.O. "Adaptive importance sampling in monte carlo integration." *Journal of Statistical Computation and Simulation* Vol. 41, No. 3-4 (1992): pp. 143–168. DOI 10.1080/00949659208810398.

[13] Wouters, J and Bouchet, F. "Rare event computation in deterministic chaotic systems using genealogical particle analysis." *Journal of Physics A: Mathematical and Theoretical* Vol. 49, No. 37 (2016): p. 374002. DOI 10.1088/1751-8113/49/37/374002.

[14] Bouchet, F., Rolland, J. and Wouters, J. "Rare Event Sampling Methods." *Chaos: An Interdisciplinary Journal of Nonlinear Science* Vol. 29, No. 8 (2019): p. 080402. DOI 10.1063/1.5120509.

[15] Ziehn, T. and Tomlin, A. S. "A global sensitivity study of sulfur chemistry in a premixed methane flame model using HDMR." *International Journal of Chemical Kinetics* Vol. 40, No. 11 (2008): pp. 742–753. DOI 10.1002/kin.20367.

[16] Najm, Habib N. "Uncertainty Quantification and Polynomial Chaos Techniques in Computational Fluid Dynamics." *Annual Review of Fluid Mechanics* Vol. 41, No. 1 (2009): pp. 35–52. DOI 10.1146/annurev.fluid.010908.165248.

[17] Iavarone, S., Oreluk, J., Smith, S.T., Hegde, A., Li, W., Packard, A., Frenklach, M., Smith, P.J., Contino, F. and Parente, A. "Application of Bound-to-Bound Data Collaboration approach for development and uncertainty quantification of a reduced char combustion model." *Fuel* Vol. 232 (2018): pp. 769 – 779. DOI 10.1016/j.fuel.2018.05.113.

[18] Yousefian, S., Bourque, G. and Monaghan, R.F.D. "Bayesian inference and uncertainty quantification for hydrogen-enriched and lean-premixed combustion systems." *International Journal of Hydrogen Energy* Vol. 46, No. 46 (2021): pp. 23927–23942. DOI 10.1016/j.ijhydene.2021.04.153.

[19] Yousefian, S., Bourque, G. and Monaghan, R.F.D. "Review of Hybrid Emissions Prediction Tools and Uncertainty Quantification Methods for Gas Turbine Combustion Systems." *Proceedings of the ASME Turbo Expo 2017: Turbomachinery Technical Conference and Exposition*: p. V04BT04A005. 2017. American Society of Mechanical Engineers, Charlotte, North Carolina, USA. DOI 10.1115/GT2017-64271.

[20] Smith, N.S.A. "Development of the conditional moment closure method for modelling turbulent combustion." Ph.D. thesis, University of Sydney. 1994.

[21] Mobini, K. "An investigation of the imperfectly stirred reactor modelling of recirculating combustion flows." Ph.D. thesis, University of Sydney. 1998.

[22] Mobini, K. and Bilger, R.W. "Imperfectly stirred reactor model predictions of reaction in a burner with strong recirculation." *Combustion Science and Technology* Vol. 176, No. 1 (2004): pp. 45–70. DOI 10.1080/00102200490255334.

[23] Mobini, K. and Bilger, R.W. "Parametric study of the Incompletely Stirred Reactor modeling." *Combustion and Flame* Vol. 156, No. 9 (2009): pp. 1818–1827. DOI 10.1016/j.combustflame.2009.06.017.

[24] Klimenko, A.Y. and Bilger, R.W. "Conditional moment closure for turbulent combustion." *Progress in energy and combustion science* Vol. 25, No. 6 (1999): pp. 595–687. DOI 10.1016/S0360-1285(99)00006-4.

[25] Gough, A.J., Mobini, K., Chen, Y. and Bilger, R.W. "Measurements and predictions in a confined bluff-body burner modeled as an imperfectly stirred reactor." *Proceedings of the Combustion Institute* Vol. 27, No. 2 (1998): pp. 3181–3188. DOI 10.1016/S0082-0784(98)80181-1.

[26] Trivedi, S., Gkantonas, S., Wright, Y.M., Parravicini, M., Barro, C. and Mastorakos, E. "Conditional Moment Closure Approaches for Simulating Soot and NOx in a Heavy-Duty Diesel Engine." *15th International Conference on Engines & Vehicles*. 2021. SAE International. DOI 10.4271/2021-24-0041.

[27] Gkantonas, S., Giusti, A. and Mastorakos, E. "Incompletely Stirred Reactor Network Modelling for Soot Emissions Prediction in Aero-Engine Combustors." *Proceedings of the International Workshop on Clean Combustion: Principles and Applications*. 2019. Darmstadt, Germany. DOI 10.17863/CAM.44973.

[28] Gkantonas, S., Giusti, A. and Mastorakos, E. "Incompletely Stirred Reactor Network Modeling of a Model Gas Turbine Combustor." *AIAA Scitech 2020 Forum*: pp. 2020–2087. 2020. American Institute of Aeronautics and Astronautics, Orlando, Florida. DOI 10.2514/6.2020-2087.

[29] Gkantonas, S., Foale, J.M., Giusti, A. and Mastorakos, E. "Soot Emission Simulations of a Single Sector Model Combustor Using Incompletely Stirred Reactor Network Modeling." *Journal of Engineering for Gas Turbines and Power* Vol. 142, No. 10 (2020): p. 101007. DOI 10.1115/1.4048408.

[30] Gkantonas, S. "Predicting Soot Emissions with Advanced Turbulent Reacting Flow Modelling." Ph.D. thesis, University of Cambridge. 2021.

[31] Iavarone, S., Gkantonas, S. and Mastorakos, E. "Incompletely Stirred Reactor Network Modeling for the Estimation of Turbulent Non-Premixed Autoignition." *International Colloquium on the Dynamics of Explosions and Reactive Systems (ICDERS)*. June 19 – 24, 2022. Naples, Italy [submitted].

[32] Gkantonas, S., Jella, S., Iavarone, S., Versailles, P., Mastorakos, E. and Bourque, G. "Estimations of Autoignition Propensity in Aeroderivative Gas Turbine Premixers Using Incompletely Stirred Reactor Network Modelling." *ASME Turbo Expo 2022: Turbomachinery Technical Conference and Exposition*. 2022. Rotterdam, The Netherlands [submitted].

[33] Jones, W.P. and Navarro-Martinez, S. "Study of hydrogen auto-ignition in a turbulent air co-flow using a Large Eddy Simulation approach." *Computers & Fluids* Vol. 37, No. 7 (2008): pp. 802–808. DOI 10.1016/j.compfluid.2007.02.015.

[34] Stanković, I., Triantafyllidis, A., Mastorakos, E., Lacor, C. and Merci, B. "Simulation of Hydrogen Auto-Ignition in a Turbulent Co-flow of Heated Air with LES and CMC Approach." *Flow, Turbulence and Combustion* Vol. 86, No. 3 (2011): pp. 689–710. DOI 10.1007/s10494-010-9277-0.

[35] Navarro-Martinez, S. and Kronenburg, A. "Flame Stabilization Mechanisms in Lifted Flames." *Flow, Turbulence and Combustion* Vol. 87, No. 2 (2011): pp. 377–406. DOI https://doi.org/10.1007/s10494-010-9320-1.

[36] Buckrell, A. J. M. and Devaud, C. B. "Investigation of Mixing Models and Conditional Moment Closure Applied to Autoignition of Hydrogen Jets." *Flow, Turbulence and Combustion* Vol. 90, No. 3 (2013): pp. 621–644. DOI 10.1007/s10494-013-9445-0.

[37] Chen, J.-Y. "Stochastic Modeling of Partially Stirred Reactors." *Combustion Science and Technology* Vol. 122, No. 1-6 (1997): pp. 63–94. DOI 10.1080/00102209708935605.

[38] Peters, N. "Laminar diffusion flamelet models in non-premixed turbulent combustion." *Progress in energy and combustion science* Vol. 10, No. 3 (1984): pp. 319–339. DOI 10.1016/0360-1285(84)90114-X.

[39] Mortensen, M. "Consistent Modeling of Scalar Mixing for Presumed, Multiple Parameter Probability Density Functions." *Physics of Fluids* Vol. 17, No. 1 (2005): p. 018106. DOI 10.1063/1.1829311.

[40] Devaud, C. B., Bilger, R. W. and Liu, T. "A New Method of Modeling the Conditional Scalar Dissipation Rate." *Physics of Fluids* Vol. 16, No. 6 (2004): pp. 2004–2011. DOI 10.1063/1.1699108.

[41] Brown, P.N. and Hindmarsh, A.C. "Reduced storage matrix methods in stiff ODE systems." *Applied Mathemat-*

ics and Computation Vol. 31 (1989): pp. 40–91. DOI 10.1016/0096-3003(89)90110-0.

[42] O'Brien, E.E. and Jiang, T.-L. "The conditional dissipation rate of an initially binary scalar in homogeneous turbulence." *Physics of Fluids A: Fluid Dynamics* Vol. 3, No. 12 (1991): pp. 3121–3123. DOI 10.1063/1.858127.

[43] Wright, Y., Depaola, G., Boulouchos, K. and Mastorakos, E. "Simulations of Spray Autoignition and Flame Establishment with Two-Dimensional CMC." *Combustion and Flame* Vol. 143, No. 4 (2005): pp. 402–419. DOI 10.1016/j.combustflame.2005.08.022.

[44] Scarinci, T., Freeman, C. and Day, I. "Passive Control of Combustion Instability in a Low Emissions Aeroderivative Gas Turbine." *Volume 1: Turbo Expo 2004*: pp. 487–499. 2004. ASMEDC, Vienna, Austria. DOI 10.1115/GT2004-53767.

[45] Nicoud, F. and Ducros, F. "Subgrid-scale stress modelling based on the square of the velocity gradient tensor." *Flow, turbulence and Combustion* Vol. 62, No. 3 (1999): pp. 183–200. DOI 10.1023/A:1009995426001.

[46] Jiménez, C., Ducros, F., Cuenot, B. and Bédat, B. "Subgrid Scale Variance and Dissipation of a Scalar Field in Large Eddy Simulations." *Physics of Fluids* Vol. 13, No. 6 (2001): pp. 1748–1754. DOI 10.1063/1.1366668.

[47] Branley, N. and Jones, W.P. "Large Eddy Simulation of a Turbulent Non-Premixed Flame." *Combustion and Flame* Vol. 127, No. 1-2 (2001): pp. 1914–1934. DOI 10.1016/S0010-2180(01)00298-X.

[48] Garmory, A. and Mastorakos, E. "Capturing localised extinction in Sandia Flame F with LES–CMC." *Proceedings of the Combustion Institute* Vol. 33, No. 1 (2011): pp. 1673 – 1680. DOI 10.1016/j.proci.2010.06.065.

[49] Sitte, M. P., Turquand d'Auzay, C., Giusti, A., Mastorakos, E. and Chakraborty, N. "A-Priori Validation of Scalar Dissipation Rate Models for Turbulent Non-Premixed Flames." *Flow, Turbulence and Combustion* DOI 10.1007/s10494-020-00218-x.

[50] McKay, M. D., Beckman, R. J. and Conover, W. J. "Comparison of Three Methods for Selecting Values of Input Variables in the Analysis of Output from a Computer Code." *Technometrics* Vol. 21, No. 2 (1979): pp. 239–245. DOI 10.2307/1268522.

[51] Hassanaly, M. and Raman, V. "Classification and computation of extreme events in turbulent combustion." *Progress in Energy and Combustion Science* Vol. 87 (2021): p. 100955. DOI 10.1016/j.pecs.2021.100955.

[52] Rasmussen, C.E. and Williams, C.K.I. *Gaussian Processes for Machine Learning (Adaptive Computation and Machine Learning)*. The MIT Press (2005).

[53] Ju, Y., Reuter, C.B., Yehia, O.R., Farouk, T.I. and Won, S.H. "Dynamics of Cool Flames." *Progress in Energy and Combustion Science* Vol. 75 (2019): p. 100787. DOI 10.1016/j.pecs.2019.100787.